MEASURING THE SPIN OF GRS 1915+105 WITH RELATIVISTIC DISK REFLECTION

J. L. BLUM[1], J. M. MILLER[1], A. C. FABIAN[2], M. C. MILLER[3], J. HOMAN[4], M. VAN DER KLIS[5], E. M. CACKETT[1,6], AND R. C. REIS[2]
[1] Department of Astronomy, University of Michigan, 500 Church Street, Ann Arbor, MI 48109, USA
[2] University of Cambridge, Institute of Astronomy, Madingley Road, Cambridge CB3 0HA, UK
[3] Department of Astronomy, University of Maryland, College Park, MD 20742, USA
[4] Kavli Institute for Astrophysics and Space Research, Massachusetts Institute of Technology, 77 Massachusetts Avenue, Cambridge, MA 02139, USA
[5] University of Amsterdam, Astronomical Inst Anton Pannekoek, Kruislann 403, NL 1098 SJ Amsterdam, Netherlands

ABSTRACT

GRS 1915+105 harbors one of the most massive known stellar black holes in the Galaxy. In 2007 May, we observed GRS 1915+105 for ∼117 ks in the low/hard state using *Suzaku*. We collected and analyzed the data with the Hard X-ray Detector/Positive Intrinsic Negative and X-ray Spectrometer cameras spanning the energy range from 2.3 to 55 keV. Fits to the spectra with simple models reveal strong disk reflection through an Fe K emission line and a Compton backscattering hump. We report constraints on the spin parameter of the black hole in GRS 1915 + 105 using relativistic disk reflection models. The model for the soft X-ray spectrum (i.e., < 10 keV) suggests $\hat{a} = 0.56^{+0.02}_{-0.02}$ and excludes zero spin at the 4σ level of confidence. The model for the full broadband spectrum suggests that the spin may be higher, $\hat{a} = 0.98^{+0.01}_{-0.01}$ (1σ confidence), and again excludes zero spin at the 2σ level of confidence. We discuss these results in the context of other spin constraints and inner disk studies in GRS 1915 + 105.

Key words: accretion, accretion disks – black hole physics – stars: individual (GRS 1915+105) – X-rays: binaries

1. INTRODUCTION

GRS 1915+105 was discovered by the WATCH instrument on board the *Granat* satellite on 1992 August 15 (Castro-Tirado et al. 1992). It has since been classified as a *microquasar*: a Galactic jet source with properties similar to quasars, but on a stellar scale. The mass of the central compact object is estimated to be $14 \pm 4\ M_\odot$ (Greiner et al. 2001). The authors reported results on the optical counterpart that implied a K–M III donating star of $\sim 1.2\ M_\odot$, making GRS 1915+105 a low-mass X-ray binary. GRS 1915+105 is well known for its extreme variability across all bands of the electromagnetic spectrum (Belloni et al. 2000).

In 1998, BeppoSAX observations of GRS 1915+105 showed the clear presence of a broad emission line at 6.4 keV (Martocchia et al. 2002), i.e., the Fe Kα line. The Fe Kα emission line is a doublet consisting of the Kα1 and Kα2 lines at 6.404 keV and 6.391 keV. Such emission lines are likely produced by irradiation of the accretion disk by an external source of hard X-rays (an external X-ray source is required because accretion disks do not efficiently self-irradiate). It is generally thought that hard X-rays originate in a hot, diffuse corona that inverse-Compton scatters soft X-ray photons emitted by the accretion disk. Irradiation of the dense disk material by the hard X-rays then gives rise to a characteristic "reflection" spectrum that results from Compton scattering and photoelectric absorption (George & Fabian 1991). Photoelectric absorption within the disk leads to the formation of the fluorescent iron emission line at about 6.4 keV. In stellar-mass black holes, highly ionized iron lines are typically observed (Miller 2007). Because of its large cosmic abundance and high fluorescent yield, the Fe Kα line is the most prominent line in the X-ray reflection spectrum.

Disk reflection is an important diagnostic of black hole spacetime geometry and general relativistic (GR) effects (e.g.,

Fabian et al. 1989; Laor 1991; Brenneman & Reynolds 2006). It is believed that the iron line originates in the innermost parts of the accretion disk and thus is highly distorted by Newtonian, special relativistic beaming, and GR effects (e.g., Fabian et al. 2000). This skewing explains the broad, skewed iron line profile that is observed in some stellar-mass X-ray binaries, such as Cygnus X-1 and GRS 1915+105 (see Miller 2007).

In our modeling of the X-ray spectrum, we make the assumption that the accretion disk extends down to the innermost stable circular orbit (ISCO) in the low/hard state. This may seem contrary to some models, in which the low/hard state is characterized by an inner disk boundary that is outside the ISCO. However, several pieces of evidence suggest that our assumption is likely to be accurate for GRS 1915+105. As follows, we observed GRS 1915+105 in the low/hard state, which is characterized by an energy spectrum that is dominated by a power-law-like component. While there is a typical photon index of ∼1.6 and a high-energy cutoff at ∼100 keV (Fender & Belloni 2004), there is also a very weak soft X-ray component (most likely associated with a thermal disk; Miller et al. 2006a). According to Nowak (1995), the total X-ray luminosity for systems in the low/hard state where distance and mass estimates are known is generally below 10% of the Eddington luminosity. Esin et al. (1997) gave an archetypal model of how accretion flows change with the state. In that model, the inner disk in the low/hard state is radially truncated at low-mass accretion rates (corresponding to $L_X/L_{\rm EDD} \leqslant 0.008$) and an advection-dominated accretion flow is present. However, the luminosity observed in GRS 1915+105 ($L \sim 0.30 L_{\rm EDD}$) is higher than what is theoretically calculated for a truncated disk in the low/hard state (Esin et al. 1997). This higher luminosity, and therefore higher mass accretion rate, is indicative of the inner disk extending closer to the black hole (e.g., Esin et al. 1997; Figure 1) and supports the notion that radially recessed disks in the low hard state may not always be the case. Recent analyses of GX 339-4, Cygnus X-1, SWIFT J1753.5-0127, and XTE
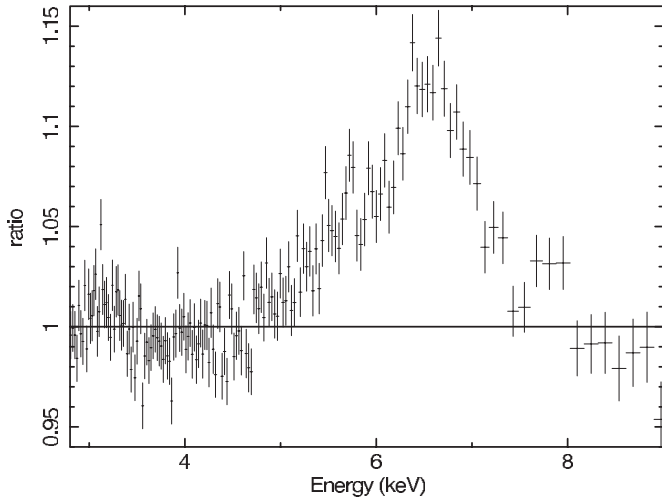
Figure 1. Data/model ratio obtained when the XIS 1 *Suzaku* spectrum of GRS 1915+105 was fit with a simple power-law model: `phabs*(powerlaw)` that included photoelectric absorption. The 4.0–7.0 keV region was ignored when fitting the model. An asymmetric skewed line profile is evident in the way predicted for relativistic lines.

J1817-330 have also revealed cool accretion disks that appear to remain close to the black hole at low accretion rates (Miller et al. 2006a, 2006b; Rykoff et al. 2007; Tomsick et al. 2008).

The radius of the ISCO is determined by the spin of the black hole: $r_{ISCO} = 6.0 \, r_g$ for $\hat{a} = 0$, and $r_{ISCO} = 1.25 \, r_g$ for an astrophysical maximum of $\hat{a} = 0.998$ (where $r_g = GM/c^2$ and $\hat{a} = cJ/GM^2$; see Thorne 1974 and Bardeen et al. 1972). The location of the ISCO determines the "strength" of the gravitational effects on the Fe K emission line (and the broadband reflection spectrum), thereby influencing how broad and skewed the line profile becomes. Therefore, determining the ISCO through line fitting serves as an indirect measure of the black hole spin parameter.

Spectral fits to thermal emission from the accretion disk in black hole binaries provide an independent way to constrain black hole spin. In order to turn the flux observed from the disk continuum into a radius (and therefore a spin parameter), the source distance, inclination, and mass must be known. In addition, factors like the line-of-sight absorption, hardening due to scattering in the disk atmosphere, and the form of the hard spectral component can be important. In order to obtain reliable spin estimates using the continuum method, it is crucial for the source to have a strong thermal component (e.g., McClintock & Remillard 2009). For the case of GRS 1915+105, this thermal component is most easily observed while in the high/soft state. However, prior spin results that have been reported for GRS 1915 + 105 in this state are not consistent. McClintock et al. (2006) and Middleton et al. (2006) both used models for thermal continuum emission from the accretion disk to calculate values of $\hat{a} > 0.98$ and $0.72^{+0.01}_{-0.02}$, respectively. In this paper, we present an independent analysis using the relativistic disk reflection spectrum to calculate the black hole spin in GRS 1915+105 in the low/hard state with the advanced cameras on *Suzaku*.

2. DATA REDUCTION

Suzaku observed GRS 1915+105 on 2007 May 7 starting at 14:40:22 (TT). The observation duration was approximately 117 ks. The X-ray Spectrometer (XIS) pointing position was used. In order to prevent photon pileup, the XIS cameras were operated using the 1/4 window mode using a 1.0 s burst option.

The XIS1 and Hard X-ray Detector (HXD)/Positive Intrinsic Negative (PIN) cameras were used in this analysis. Two other XIS units were turned off to preserve telemetry, and the fourth unit was run in a special timing mode (which has yet to be calibrated). XIS on-source times of approximately 51 ks were achieved. This resulted in a dead-time corrected net exposure of 25 ks for the XIS1 camera (in the 3×3 editing mode). A net exposure time of 57 ks was achieved using the HXD/PIN.

For the soft X-ray data, the 2.3–10 keV energy range was used in order to avoid calibration problems near the Si K edge and because there are few photons at low energy owing to high line-of-sight absorption ($n_H \sim 4.0 \times 10^{22}$ cm^{-2}). Using the clean event file (3×3 mode data) with the latest calibration databases at the time from the XIS data (CALDB 20070731: version 2.0.6.13), we extracted the source light curve and spectrum with `xselect`. An annulus centered on the source with an inner radius of $78''$ and an outer radius of $208''$ (75 and 200 in pixel units, respectively) was used for the source extraction region because the center of the image suffered pileup. An annulus centered on the source was also used for the background extraction region with an inner radius of $208''$ and an outer radius of $271''$ (200 and 260 in pixel units, respectively). We manually corrected for extracted region areas that did not land on the XIS chip. The XIS redistribution matrix files (RMFs) and ancillary response files (ARFs) were created using the tools `xisrmfgen` and `xissimarfgen` available in the HEASOFT version 6.6.2 data reduction package. The 3×3 mode event file was used to specify good time intervals and the data were grouped to a minimum of 25 counts per bin using the FTOOL `grppha`.

For the HXD data, the latest calibration databases (CALDB 20070710) were used and the reduction process began with a clean event file from the PIN detector (energy range 10.0–70.0 keV), which was at XIS aim point. In the PIN data reduction process, the PIN spectrum was extracted and dead time was corrected by using the pseudoevents files. After the non-X-ray background (NXB) spectrum was extracted, the exposure time of the background spectrum was increased by a factor of 10 since the NXB event file was calculated with a count rate 10 times higher than the real background count rate to reduce statistical errors. The cosmic X-ray background was simulated, modeled and added to the NXB spectrum in XSPEC version 12.5.0 as instructed in the *Suzaku* ABC guide.

3. DATA ANALYSIS AND RESULTS

Using the X-ray spectral fitting software package (XSPEC v. 12.5.0; Arnaud 1996), we initially fit the *Suzaku* XIS spectrum of GRS 1915 + 105 with a simple absorbed power-law model: `phabs*(powerlaw)`, with the `phabs` model component accounting for Galactic photoelectric absorption. All parameters were allowed to vary. The 4.0–7.0 keV range was ignored when fitting the data to obtain an unbiased view of the Fe K range. The fit resulted in an equivalent hydrogen column, n_H, of $4.51^{+0.06}_{-0.06}$ (in units of 10^{22} cm^{-2}) and a photon index, Γ, of $2.09^{+0.01}_{-0.01}$ ($\chi^2/\nu = 1402/1282$). That ignored energy range was then restored when forming the data/model ratio as shown in Figure 1. An asymmetric, skewed line is revealed in the exact way predicted for relativistic disk lines. In a similar manner, Figure 2 shows the XIS and HXD spectra fit with a simple model consisting of a broken power law modified by interstellar absorption: `phabs*(bknpow)`. A constant was allowed to float between the two data sets. The 4.0–7.0 keV and 15.0–45.0 keV ranges were ignored when fitting in order to
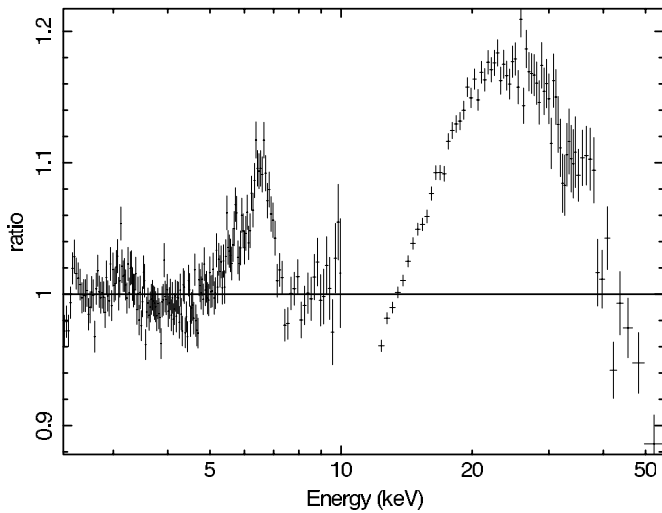
Figure 2. Data/model ratio obtained when the XIS and HXD *Suzaku* spectra of GRS 1915+105 were fitted with a broken power-law model: `phabs*(bknpow)` that included photoelectric absorption. For the HXD spectra, the model was fit over the 12.0–15.0 keV and 45.0–55.0 keV energy ranges. The 4.0–7.0 keV and 15.0–45.0 keV regions were ignored when fitting the model. The residuals near 12 keV can be attributed to calibration problems near the edge of the detector. The curvature at high energy is a clear signature of disk reflection.

Figure 3. Best-fit spectrum found through modeling of the iron line at 6.4 keV. Model: `phabs*(kerrdisk + kerrconv*pexriv)`.

properly model the continuum. Note that for the HXD spectra, the model was fit over the 12.0–15.0 keV and 45.0–55.0 keV energy ranges. The fit resulted in $n_H = 4.35^{+0.06}_{-0.07}$, $\Gamma_1 = 2.03^{+0.02}_{-0.02}$, and $\Gamma_2 = 2.59^{+0.02}_{-0.02}$ with an energy break at $7.7^{+0.2}_{-0.2}$ keV ($\chi^2/\nu = 1565/1312$). Again, the ignored energy ranges were restored when forming the data/model ratio. Note that the residuals near 12 keV can be attributed to calibration problems near the edge of the detector.

XSPEC provides a number of models for spectral line fitting. Models of particular interest to us not only allow for analysis of the observed broad iron line in our data, but account for the special and GR effects that physically go into creating such an emission profile around a black hole. Since determining the black hole spin of GRS 1915+105 through analysis of the iron line is our main priority, models that allow spin to be a free parameter in our fits are useful. Brenneman & Reynolds (2006) have calculated models (`kerrdisk` and `kerrconv`) that describe line emission from an accretion disk and include black hole spin as a free parameter, thereby allowing us to formally constrain the angular momentum of the black hole and other physical parameters of the system. The `kerrdisk` model describes line emission from an accretion disk, while the `kerrconv` model allows one to convolve a reflection spectrum with the smeared line function.

Although general relativity permits the spin parameter $\hat{a}$ to have any arbitrary value, black holes can in principle have spin parameters $-1 \leqslant \hat{a} \leqslant 1$. However, for simplicity, the `kerrdisk` model only considers a black hole that has a prograde spin relative to the accretion disk that spins up to the Thorne (1974) spin-equilibrium limit, i.e., $0 \leqslant \hat{a} \leqslant 0.998$.

In addition to the spin parameter, we can specify and/ or constrain nine other physical parameters in the `kerrdisk` model: (1) rest-frame energy of the line; (2) emissivity index within a specified radius; (3) emissivity index at radii larger than a specified value; (4) break radius separating the inner and outer portions of the disk (in units of gravitational radii); (5) the disk inclination angle to the line of sight; (6) the inner radius of the disk in units of the radius of marginal stability (rms); (7) the
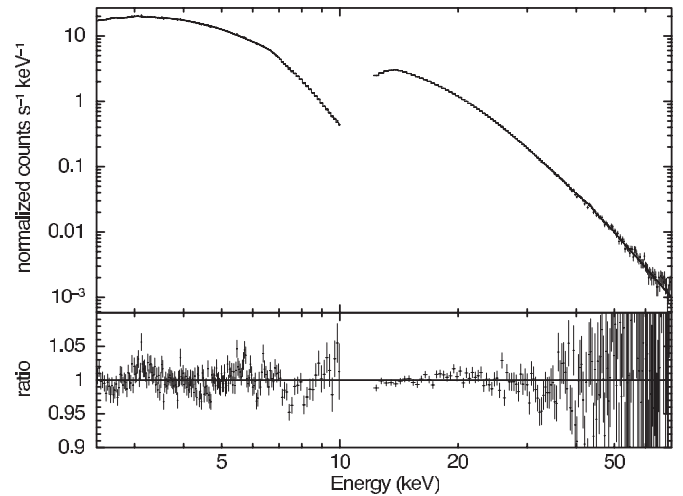
outer radius under consideration; (8) the cosmological redshift of the source ($z = 0$ for our source); and (9) the normalization (flux) of the line in photons cm^{-2} s^{-1}. `kerrconv` has the same basic set of parameters with the exception that it does not require an input line energy or a flux normalization parameter since it uses a `kerrdisk` kernel to smear the entire spectrum with relativistic effects. Of these parameters, we let 1, 2, 3, 5, and 9 vary freely. We bounded the rest-frame energy for the iron line between 6.4 and 6.97 keV and the disk inclination between 55° and 75° based on the figure presented in Fender et al. (1999, Figure 6) from radio jet observations. The emissivity indices were fixed to be equal to each other meaning that we only consider one index, making the break radius meaningless. Parameters 4, 6, and 7 were frozen at 6.0 r_g, 1.0 rms, and 400 rms, respectively using the "standard" values of the `kerrdisk` and `kerrconv` models. By doing this, we assume that the ionization of the disk material within the ISCO is too high to produce significant line emission as has been shown by three-dimensional magnetohydrodynamics (MHD) simulations (Reynolds & Fabian 2008).

As shown in Figure 3, our model is defined as `phabs*(kerrdisk + kerrconv*pexriv)`. A constant was allowed to float between the XIS and HXD data sets. The model component `pexriv` is an exponentially cutoff power-law spectrum reflected from ionized material (Magdziarz & Zdziarski 1995). The free parameters are the power-law photon index Γ, the fold energy or cutoff energy (in keV), and the scaling factor for reflection. Our results are given in Table 1 with the model being fit in the 2.3–10.0 keV and 12.0–55.0 keV energy ranges. Note that the residual feature at the upper limit of the XIS detector is the result of noise. Errors were calculated using the *steppar* command in XSPEC, which affords control over how the χ^2 space is searched. For all parameters, errors refer to the 68% confidence level ($\Delta\chi^2 = 1$) unless otherwise stated. The reduced χ^2 of our best fit is 2345/2224. We measure a spin value of $\hat{a} = 0.98^{+0.01}_{-0.01}$. Figure 4 plots the dependence of χ^2 on the black hole spin parameter. A spin of zero is excluded at the 2σ level of confidence.

The disk ionization parameter ($\xi = L_X/nr^2$, where n is the hydrogen number density) has a large effect on the resulting spectrum. Ross et al. (1999) demonstrated the effect on reflection spectra models for a range of ionization values ($30 < \xi < 10^5$). The model with the highest ionization
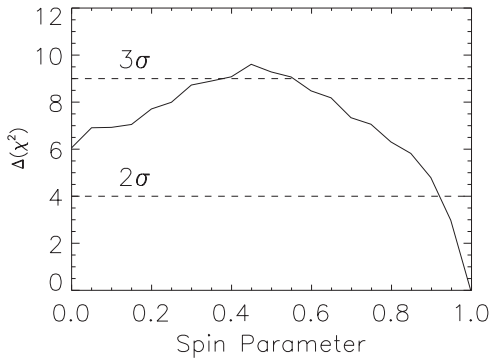
Figure 4. Above plot shows the change in the goodness-of-fit statistic as a function of the black hole spin parameter, $\hat{a}$ for the model `const.*phabs*(kerrdisk + kerrconv*pexriv)`. Using the XSPEC *steppar* command, 20 evenly spaced values of $\hat{a}$ were frozen, and all other parameters were allowed to float freely to find the best fit at that spin parameter. The dotted lines indicate confidence intervals.

Table 1
XSPEC Model

Model Component	Parameter	Value
`phabs`	nH (10^{22}) (cm^{-2})	$4.15^{+0.06}_{-0.06}$
`kerrdisk`	Fe line energy (keV)	$6.40^{+0.06}$
	rb (rms)	(6.0)
	Emissivity index	$1.8^{+0.1}_{-0.1}$
	a (cJ/GM^2)	$0.98^{+0.01}_{-0.01}$
	Inclination (deg)	$55.0^{+2.0}$
	R_i	(1.0)
	R_o	(400)
	Redshift	(0)
	Norm. (photons cm^{-2} s^{-1})	$0.010^{+.002}_{-.002}$
`pexriv`	Photon index	$1.96^{+0.03}_{-0.03}$
	Fold E (keV)	$38^{+1.0}_{-1.0}$
	Rel. reflection	$0.38^{+0.02}_{-0.02}$
	Fe/solar	(1.0)
	Cosine of inc. angle	(0.45)
	T_{disk} (K)	(300,000)
	Disk ionization (erg cm s^{-1})	(5000)
	Norm. (photons keV^{-1} cm^{-2} s^{-1})	$3.8^{+0.10}_{-0.10}$
χ^2/ν		2345/2224

Notes. These are the best-fit parameters found using the model `phabs*(kerrdisk+kerrconv*pexriv)` with the XIS and HXD data. All of the `kerrdisk` and `kerrconv` parameters were tied, and a constant was allowed to float between the XIS and HXD data sets. The errors quoted in Table 1 are 1σ errors unless otherwise noted. The values in parentheses were fixed during the fitting. The calculated luminosity (0.5–100 keV; 10^{38}erg s^{-1}) for a distance $d \sim 12$ kpc (Fender & Belloni 2004) is $5.7^{+0.10}_{-0.10}$.

Figure 5. Best-fit spectrum found through modeling of the iron line at 6.4 keV. Model: `phabs*(powerlaw + kerrconv*reflionx)`.

parameter, $\xi = 10^5$, was the best reflector but had negligible iron spectral features due to the disk surface layer being fully ionized at great depth, with the iron line (specifically, Fe XXVI) not becoming dominant until $\tau \approx 8$. However, when ξ is reduced to 3×10^3, less than half of the iron is fully ionized at the disk's surface and Fe XXV becomes dominant at $\tau \approx 1$. Most importantly, at this value an iron emission line that is Compton-broadened becomes visible (Ross et al. 1999, Figure 2). Similar to this ionization value is our value of 5000, which is the upper limit allowed by the `pexriv` model. This "high" value was chosen so as to obtain the maximum amount of broadening due to Comptonization and further understand the dynamics of the system. In our model, maximizing or minimizing the disk temperature (10^6 and 10^4 K, respectively) changed χ^2 by less than 5, resulting in similar reduced χ^2 to the best-fit value
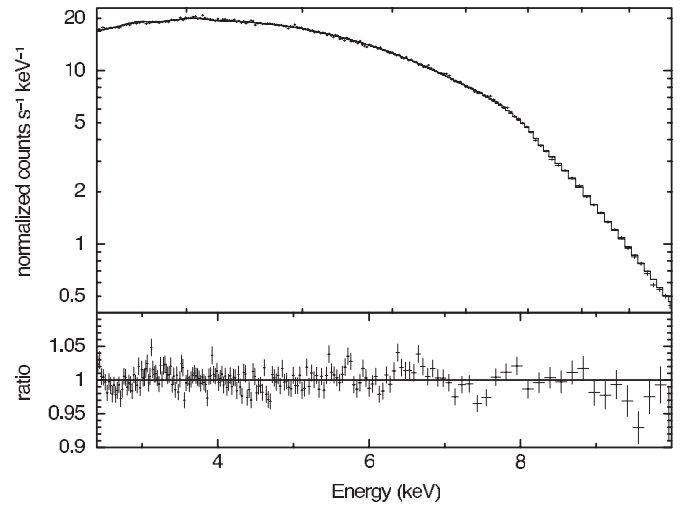
($\chi^2/\nu \sim 1.05$). Effects to the parameter values (most notably the spin parameter) were negligible with the exception of the reflection scaling factor, which changed by < 0.06. Note that a thermal disk component is not required for our model and, since the disk itself is likely to be relatively cool and the high Galactic photoelectric absorption prevents its detection, we have set a low disk temperature (see, e.g., Miller et al. 2006a; Rykoff et al. 2007).

Given the complexity of the source and its extreme variability, we had set the iron abundance equal to the solar value to provide a more simplistic approach to constraining the spin, our main parameter of interest. Using the upper limit on the ionization value we tested the effects of altering the iron abundance in the `pexriv` model. Ross & Fabian (2005, Figure 5) showed that increasing the iron abundance relative to the solar value serves to lower the continuum while enhancing the Fe Kα emission lines. Additionally, Lee et al. (2002) measured an iron abundance, Fe/solar, > 1.0 for GRS 1915+105, conveying that the overabundance may be due to dynamics of supernova in the microquasar's history. However, Ueda et al. (2009) were more definitive in fitting a spectrum with better statistics using solar values for the abundances (including iron). As such, after testing the effects of varying abundance, our `pexriv` model did not require an enhanced abundance (e.g., tripling the iron abundance increased χ^2 by ~ 100).

Our broadband model uses `pexriv` as its main reflection component. One difficulty with this model is that it does not include the effects of Comptonization on photoelectric absorption edges in the outer, most highly ionized layers of the disk. Being statistically inferior in this regime, it may not be ideal to use this model for high values of ξ, which is the reason that our value of 5000 erg cm s^{-1} is the upper limit. In order to check how our spin constraints might depend on the reflection model, we replaced `pexriv` with a newer, more self-consistent reflection model: `reflionx` (see Figure 5). The `reflionx` model is a revised version of `reflion` (Ross & Fabian 2005) that describes reflection from accretion disks in black hole systems where the blackbody emission is at too low an energy to affect the Fe Kα emission. It has been used previously to constrain the spin in other sources such as GX 339-4 (Reis et al. 2008). The parameters of the model are the iron abundance (set to solar), photon index of the illuminating power law, ionization

Table 2
XSPEC reflionx Model

Model Component	Parameter	Value
phabs	nH (10^{22}) (cm^{-2})	$5.64^{+0.03}_{-0.03}$
powerlaw	Gamma	$2.44^{+0.01}_{-0.01}$
	Normalization	$6.78^{+0.03}_{-0.03}$
kerrconv	Index	$2.1^{+0.1}_{-0.1}$
	rb (rms)	(6.0)
	a (cJ/GM^2)	$0.56^{+0.02}_{-0.02}$
	Inclination (deg)	$69.3^{+2.0}_{-2.0}$
	R_i	(1.0)
	R_o	(400)
reflionx	Fe/solar	(1.0)
	Gamma	$2.44^{+0.01}_{-0.01}$
	χ_i	$100^{+3.0}_{-3.0}$
	Redshift	(0)
	Normalization (10^{-3})	$2.5^{+0.3}_{-0.3}$
χ^2/ν		2124/2100

Notes. These are the best-fit parameters found using the `phabs*(powerlaw+kerrconv*reflionx)` model with only XIS data. The errors quoted are 1σ errors unless otherwise noted. The values denoted in parentheses are fixed parameters.

parameter, ξ, and the normalization. In fitting `reflionx`, the HXD spectrum was neglected because a cutoff power law is required whereas `reflionx` assumes that a simple power-law spectrum irradiates the disk. Moreover, `reflionx` is a pure reflection model that requires a simple power law to represent the continuum. Note that the Fe K emission line is self-consistently modeled within the `reflionx` model. Also, in order to obtain better constraints within the `reflionx` model, the inclination was bounded between at $55°$ and $75°$. The model was fit in the 2.3–10.0 keV energy range. Letting $\hat{a}$ be a free parameter, the `phabs*(powerlaw+kerrconv*reflionx)` model resulted in a spin parameter of 0.56 with a χ^2 value of approximately 2124 and a reduced $\chi^2 \sim 1.01$ for 2100 degrees of freedom (see Table 2). Based on these results from the `reflionx` model, we can state that $\hat{a} = 0.56^{+0.02}_{-0.02}$ is preferred and that a spin of zero is excluded at the 4σ level of confidence (see Figure 6). However, it is important to note that the parameter values obtained with the `reflionx` model are poorly constrained, which requires the `pexriv` results to be viewed with extra caution (see Section 4).

Finally, we note the possible presence of an absorption line at approximately 7.4 keV (see Figure 1). It is not clear that the feature is real. When the broadband spectrum is fit phenomenologically, a Gaussian model for the line suggests a (single-trial) significance of 4σ. The feature is not significant after fitting the relativistic emission line and disk reflection continuum. If the line is real, it could plausibly be associated with Fe xxv or Fe xxvi, implying a wind with a blueshift as high as $0.1c$. When a strong line is frozen as part of the overall spectral model, even modest constraints on the spin parameter of the black hole cannot be obtained. However, a wind in a hard state would be inconsistent with an apparent anti-correlation between winds and jets in GRS 1915 + 105 (Miller et al. 2008a; Neilsen & Lee 2009).

4. DISCUSSION

In this paper, we have presented the first results from *Suzaku* observations of GRS 1915 + 105 in a low/hard state. We have observed the Fe K emission line in GRS 1915+105 in unprecedented detail due to the spectral resolution and fast
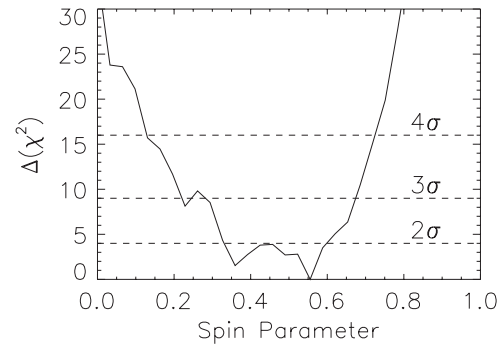

Figure 6. Above plot shows the change in the goodness-of-fit statistic as a function of the black hole spin parameter, $\hat{a}$ for the model `phabs*(powerlaw+kerrconv*reflionx)`. Using the XSPEC *steppar* command, 30 evenly spaced values of $\hat{a}$ were frozen and all other parameters were allowed to float freely to find the best fit at that spin parameter. The dotted lines indicate confidence intervals. Note that only the XIS data were used in this model.

readout modes of the XIS cameras. Our broadband spectral model suggests a spin of $\hat{a} = 0.98^{+0.01}_{-0.01}$, though a value of zero is only excluded at the 2σ level of confidence. A different model, fitted only to the soft X-ray spectrum, results in a spin of $\hat{a} = 0.56^{+0.02}_{-0.02}$ with a value of zero excluded at 4σ level of confidence. This effort to measure the spin of the black hole in GRS 1915 + 105 follows other recent efforts to measure spin in stellar-mass black holes using relativistic iron lines (Miller et al. 2008b; Reis et al. 2008, 2009; Miller et al. 2009) and the thermal disk continuum spectrum (e.g., Shafee et al. 2006).

Owing to its extreme behavior and the possibility of a relation to the spin of the black hole, it is particularly important to understand the black hole in GRS 1915 + 105. Middleton et al. (2006) and McClintock et al. (2006) used similar thermal emission continuum models based on different data selections from *Rossi X-Ray Timing Explorer* (*RXTE*) to estimate the spin of the black hole in GRS 1915 + 105. Middleton et al. (2006) determined the spin of GRS 1915+105 from a set of 16 *RXTE* observations (approximately spanning from 1994 to 1996) that were 16 s each. The authors chose spectra where there was a slow change between spectral states, specifically variability classes β and λ (Belloni et al. 2000), which is why short timescale spectral binning was used. They required that Comptonization contribute less than 15% of the bolometric flux (or rather that the disk contributed greater than 85%). Also, the rms variability had to be < 5%. For the final analysis, there were a total of 34 disk dominated spectra for six observations. The XSPEC models used were for a multicolor disk blackbody (`diskbb`), relativistic effects (`bhspec`), and thermal Comptonization (`thcomp`) that result in an intermediate spin value of $\hat{a} = 0.72^{+0.01}_{-0.02}$

For comparison, McClintock et al. (2006) used a much larger sample of *RXTE* data than Middleton et al. (2006) with a total observation time of 89 ks for *RXTE* and 13 ks for *ASCA*. The 22 observations selected had to meet three criteria: (1) weak QPOs; (2) rms continuum power < 0.075 rms; and a (3) disk flux > 75% of the total 2–20 keV emission. The authors used a relativistic disk model (`kerrbb2`: a combination of `kerrbb` and `bhspec` that included a spectral hardening factor), which would alternately be combined with a power law, Comptonization (`comptt`), and a cutoff power-law model (`cutoffpl`). These last three models represented the nonthermal tail component of the emission. They argued that the spin ($\hat{a} > 0.98$) and mass accretion rate parameters were relatively unaffected by the model for the nonthermal tail component.

Both sets of authors have identified several reasons that might explain the different spin values that they derived. McClintock et al. (2006) noted the existence of uncertainties in disk structure at high luminosities. These uncertainties could possibly affect the Middleton et al. (2006) results, which used solely high-luminosity observations ($L > 0.3\ L_{EDD}$). McClintock et al. (2006) also suggested that Middleton et al. (2006) missed crucial low-luminosity observations because of small data samples—the derived intermediate spin value may be due to averaging over a wide range of luminosities (including a super-Eddington luminosity of $L \sim 1.45\ L_{EDD}$). However, Middleton et al. (2006) suggested that the McClintock et al. (2006) low-luminosity data ($L < 0.3\ L_{EDD}$) do not allow for a low-temperature Comptonized component ($kT_e < 3$ keV).

In summary, McClintock et al. (2006) found a rapidly spinning black hole in GRS 1915+105 based on *disk continuum* fits from *RXTE* and *ASCA* data. Middleton et al. 2006) used similar assumptions (i.e., $d \sim 12$ kpc and inclination angle $\sim 66°$ (Fender et al. 1999)) and models, but had a smaller sample of *RXTE* data of GRS 1915+105 and obtained an intermediate value of $\hat{a} = 0.72^{+0.01}_{-0.02}$. The behavior of GRS 1915 + 105 is particularly complex and the states identified in this source are more numerous and nuanced than those identified in other black hole binaries. The differences in Middleton et al. (2006) can partly be attributed to the state classifications (i.e., A, B, C) for GRS 1915+105 as opposed to the black hole binary categories used by McClintock et al. (2006). The spin estimate reported by McClintock et al. (2006) was obtained in a state that resembles the "thermal state" (i.e., high/soft state or "thermal dominant" state). Here, our observation was obtained in the low/hard state (which is mostly likely "state C").

Previous work has suggested that for non-spinning black holes, the amount of Fe K emission from within the ISCO is negligible: inside the ISCO, the ionization fraction sufficiently increases close to the black hole making it unlikely that there is significant Fe K emission within the ISCO since the ionization fraction substantially increases (Reynolds & Begelman 1997). Reynolds & Fabian (2008) found that systematic errors on the spin due to emission from within the ISCO become smaller for more rapidly rotating black holes. Additionally, Shafee et al. (2008) determined that magnetic coupling is unimportant across the ISCO for geometrically thin disks. The best current theoretical works suggest that systematic errors are unlikely to bias our results for GRS 1915+105 (Reynolds & Fabian 2008).

An r^{-3} disk emissivity relation is typically assumed for line emission from a standard thin accretion disk with an isotropic source of disk irradiation (see, e.g., Reynolds & Nowak 2003). Freezing the emissivity index at 3.0 in the pexriv and reflionx models resulted in worse fits with $\Delta\chi^2 \gtrsim 200$ for 1 degree of freedom (*F*-value >180, $> 8.0\sigma$ level of confidence). Our current best-fit value for the emissivity index in GRS 1915+105 is of interest because it implies that the reflected emission has a weaker dependence on the radius ($r^{-2.0}$) than is typical. When the emissivity index is high, as in the case for many spinning active galactic nuclei, there is significant iron line flux below 4 keV from material closest to the black hole and therefore high gravitational redshift. This is not true when the emissivity index is low. Thus, spin determination for the GRS 1915+105 case is being driven more by the detailed shape of the body of the iron line rather than the overall line extent. This could explain much of the difference between the pexriv and reflionx results. Moreover, a stable warp at the inner disk (e.g., due to Lense–Thirring precession) is a possible explanation for our different emissivity index value in that it would reflect more than expected at larger radii. A link between Fe K emission and the phase of low-frequency quasi-periodic oscillations (QPOs) in the low/hard state of GRS 1915 + 105 may provide evidence for such a warp (Miller & Homan 2005).

Martocchia et al. (2006) made two *XMM-Newton* observations of GRS 1915+105 in 2004 during a long "plateau" (lower flux) state. The data were analyzed with EPIC-pn in timing and burst modes, respectively. For the timing mode, they detected a broad excess at the energy of the iron line and fit the data from 2.0 to 10.0 keV with the disk reflection model diskline (Fabian et al. 1989). Martocchia et al. (2006) found an inner radius of the disk in excess of 300 R_g for an unabsorbed flux of 1.0 $\pm$ 0.1 (10^{-8} erg s^{-1} cm^{-2}) in the 2.0–10.0 keV energy range. Although such a disk would have the advantage of providing a geometric explanation for the major X-ray spectral transitions seen in Galactic black holes (Done & Gierliński 2006), the high (unabsorbed) flux ($\sim 3.3 \times 10^{-8}$erg s^{-1} cm^{-2}) and hence high luminosity ($\sim 0.30\ L_{EDD}$) we calculated in the 0.5–100 keV range for GRS 1915+105 make it unlikely that the disk would be recessed to such a high value (e.g., Esin et al. 1997; Frank et al. 2002, p. 152; also see Miller et al. 2006a). We note that the high flux of GRS 1915+105 may have caused photon pileup in the EPIC-pn timing mode, thereby obscuring the breadth of the line and affecting the Martocchia et al. (2006) results.

Based on Very Large Array (VLA) observations of relativistic ejections from GRS 1915+105, $70° \pm 2°$ is the typical value used for the inclination of this source (Mirabel & Rodríguez 1994). However, in our broadband model the inclination angle pegged at $55°$, which is close to the lowest plausible value for this black hole binary (we set the bounds between $55°$ and $75°$; Fender et al. 1999, Figure 6). Allowing the inclination to vary over a greater range ($20°$–$80°$) resulted in our broadband model finding the minimum χ^2 at $40°$, which we disregard on the basis that it is not consistent with previous radio jet observations (e.g., Mirabel & Rodríguez 1994; Fender et al. 1999). Given our assumption that the spin axis of the black hole is parallel to the jet axis, our best-fit spin and inclination results follow from self-consistent assumptions.

As mentioned previously, the resulting parameter values in the reflionx model are not well constrained. To better demonstrate the dependence between parameters, particularly for the spin parameter, Figures 7 and 8 show the 68%, 90%, and 99% contour plots for inclination versus spin for both the reflionx and pexriv models, respectively. As shown for the reflionx model, there is a large degree of variation between the inclination and spin values whereas for the pexriv model, the spin and inclination values are more restricted. Due to the poor constraints in the reflionx model, the pexriv model results must be regarded with more caution.

Among stellar-mass black holes, GRS 1915 + 105 displays uniquely rich and complex phenomena, both in X-rays and at shorter wavelengths. Its X-ray spectrum is similarly complex, and whether using the disk continuum or the reflection spectrum to constrain the spin, data selection and modeling nuances can be important. Currently, our broadband model (pexriv) gives a spin parameter that is in agreement with the value reported by McClintock et al. (2006; $\hat{a} > 0.98$), while the upper limit on our soft X-ray spectrum model (reflionx) spin result is lower than the Middleton et al. (2006) spin value. In this effort to constrain the spin of GRS 1915 + 105, we have considered only a single observation in a single state, though disk reflection is sure to
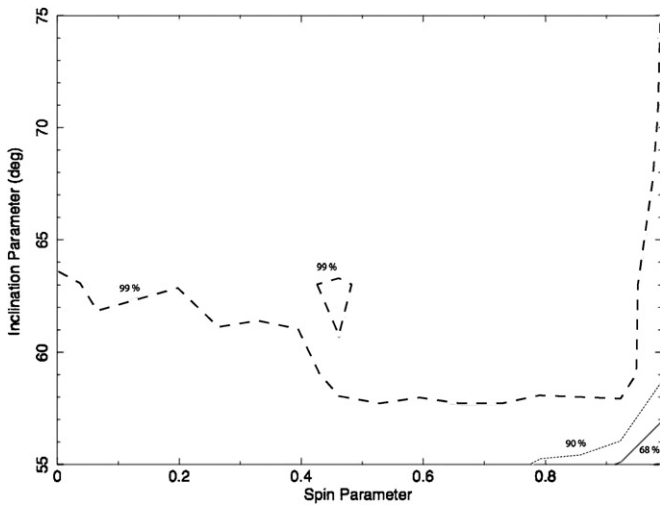
Figure 7. Inclination vs. spin contour plot for GRS 1915+105 using the `pexriv` model. The solid, dotted, and dashed lines show the 68%, 90%, and 99% confidence range for two parameters of interest, respectively.
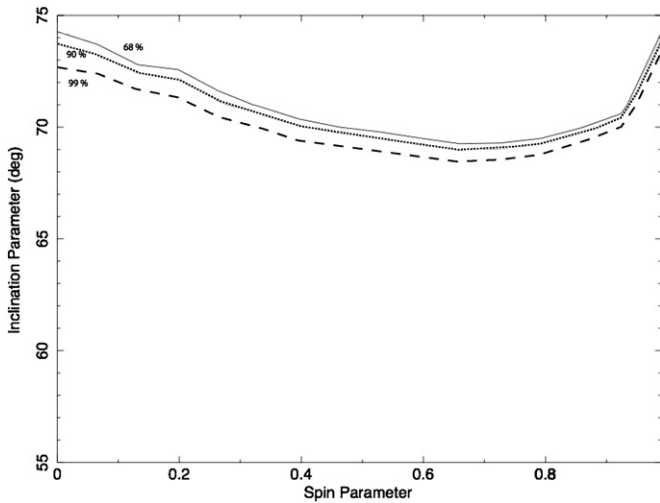

Figure 8. Inclination vs. spin contour plot for GRS 1915+105 using the `reflionx` model. The solid, dotted, and dashed lines show the 68%, 90%, and 99% confidence range for two parameters of interest, respectively.

be important in many states. Future observations with *Suzaku* and *XMM-Newton* in different states may allow the spin to be determined more clearly using the disk reflection spectrum. The thermal disk continuum is not evident in our observation, but future efforts that make joint use of the direct and reflected disk spectrum to constrain the spin (e.g., Miller et al. 2009) may provide another way forward.

REFERENCES

Arnaud, K. A. 1996, in ASP Conf. Ser. 101, Astronomical Data Analysis Software and Systems V, ed. G. H. Jacoby & J. Barnes (San Francisco, CA: ASP), 17
Bardeen, J. M., Press, W. H., & Teukolsky, S. A. 1972, ApJ, 178, 347
Belloni, T., et al. 2000, A&A, 355, 271
Brenneman, L. W., & Reynolds, C. S. 2006, ApJ, 652, 1028
Castro-Tirado, A. J., Brandt, S., & Lund, N. 1992, IAU Circ., 5590
Done, C., & Gierliński, M. 2006, MNRAS, 367, 659
Esin, A. A., McClintock, J. E., & Narayan, R. 1997, ApJ, 489, 865
Fabian, A. C., Iwasawa, K., Reynolds, C. S., & Young, A. J. 2000, PASP, 112, 1145
Fabian, A. C., et al. 1989, MNRAS, 238, 729
Fender, R., & Belloni, T. 2004, ARA&A, 42, 317
Fender, R., et al. 1999, MNRAS, 304, 865
Frank, J., King, A., & Raine, D. 2002, Accretion Power in Astrophysics (3rd. ed.; Cambridge: Cambridge Univ. Press)
George, I. M., & Fabian, A. C. 1991, MNRAS, 249, 352
Greiner, J., et al. 2001, A&A, 373, L37
Laor, A. 1991, ApJ, 376, 90
Lee, J. C., et al. 2002, ApJ, 567, 1102
Magdziarz, P., & Zdziarski, A. 1995, MNRAS, 273, 837
Martocchia, A., et al. 2002, A&A, 387, 215
Martocchia, A., et al. 2006, A&A, 448, 677
McClintock, J. E., & Remillard, R. A. 2009, Astro 2010: The Astron. and Astrophys. Decadal Survey, Science White Papers, no. 197 (arXiv:0902.3488v3)
McClintock, J. E., et al. 2006, ApJ, 652, 518
Middleton, M., et al. 2006, MNRAS, 373, 1004
Miller, J. M. 2007, ARA&A, 45, 441
Miller, J. M., & Homan, J. 2005, ApJ, 618, L107
Miller, J. M., Reynolds, C. S., Fabian, A. C., Miniutti, G., & Gallo, L. C. 2009, ApJ, 697, 900
Miller, J. M., et al. 2006a, ApJ, 653, 525
Miller, J. M., et al. 2006b, ApJ, 652, L113
Miller, J. M., et al. 2008a, ApJ, 680, 1359
Miller, J. M., et al. 2008b, ApJ, 679, L113
Mirabel, I. F., & Rodríguez, L. F. 1994, Nature, 371, 46
Neilsen, J., & Lee, J. C. 2009, Nature, 458, 481
Nowak, M. A. 1995, PASP, 107, 1207
Reis, R. C., et al. 2008, MNRAS, 387, 1489
Reis, R. C., et al. 2009, MNRAS, 395, 1257
Reynolds, C. S., & Begelman, M. C. 1997, ApJ, 488, 109R
Reynolds, C. S., & Fabian, A. C. 2008, ApJ, 675, 1048
Reynolds, C. S., & Nowak, M. A. 2003, Phys. Rep., 377, 389
Ross, R. R., & Fabian, A. C. 1999, MNRAS, 306, 461
Ross, R. R., & Fabian, A. C. 2005, MNRAS, 358, 211
Ross, R. R., Fabian, A. C., & Young, A. J. 1999, MNRAS, 306, 461
Rykoff, E., Miller, J. M., Steeghs, D., & Torres, M. A. P. 2007, ApJ, 666, 1129
Shafee, R., et al. 2006, ApJ, 636, L113
Shafee, R., et al. 2008, ApJ, 687, L25
Thorne, K. S. 1974, ApJ, 191, 507
Tomsick, J. A., et al. 2008, ApJ, 680, 593
Ueda, Y., Yamaoka, K., & Remillard, R. 2009, ApJ, 695, 888